CME LIVE OPEN ACCESS

International Journal of
Oral Health Dental Management

Research Article

ISSN: 2577-6533

Comparative Study of Stress Distribution in Tissue Surrounding Dental Implant Flexure: Continuum vs Full Body Analysis

Salah A M Elshourbagy*

Tanta university, faculty of engineering, department: production and mechanical design, Egypt.

Corresponding Author: Salah A M Elshourbagy, Tanta university, faculty of engineering, department: production and mechanical design, Egypt.

Received: 2025 Apr 29 **Accepted:** 2025 May 14 **Published:** 2025 May 28

Abstract

The use of dental implants has surged in popularity as an effective solution for individuals dealing with tooth loss. A successful dental implant must possess several essential qualities. It must be biocompatible to prevent any adverse reactions or rejection by the body. Furthermore, osseointegration, the fusion of the implant with the surrounding bone tissue, is crucial for stability and support. The implant should also demonstrate strength and durability to withstand biting and chewing forces without fracturing. Its long-lasting design is pivotal for ensuring durability over time. Additionally, the size and shape of the implant should be carefully selected to suit the patient's unique jawbone and surrounding tissues.

To deepen our comprehension of dental implant behavior, we conducted a comparative study between a full-body diagram and the traditional continuum model for implant modeling. Our investigation revealed that incorporating a full-body diagram provides a more reliable and accurate simulation of the implant's response under various loading conditions. Moreover, the adaptability in size and shape of dental implants allows for the placement of different crown shapes and sizes, preserving the aesthetic appeal of the patient's teeth. By grasping the essential characteristics of successful dental implants and utilizing advanced modeling techniques, we can improve the outcomes of dental implant procedures.

Keywords: Dental Implants, Strength, Durability, Surrounding Tissues, Full-Body Diagram, Continuum Model, Loading Conditions

1. Introduction

Dental implants play a vital role in addressing tooth loss, offering a range of advantages like enhanced aesthetics, improved oral health, and the prevention of further oral complications. Additionally, they contribute to better speech clarity, comfort, and chewing ability. By restoring both function and appearance, dental implants significantly enhance the overall quality of life, serving as a long-term solution for oral health and well-being. This research delves into the stress experienced by dental implants during rotation at various angles and aims to examine their displacements and stress distribution. The primary objective is to evaluate the capacity and durability of dental implants, ensuring a secure and effective tooth replacement system.

The distribution and magnitude of stress on dental prosthesis components vary depending on the type of mechanical loading applied [1]. Studies indicate that the new design of dental implants can reduce stress transfer to the surrounding cortical bone, thereby enhancing its long-term durability [2]. The use of short implants with long crowns may potentially lead to biomechanical complications and an increased risk of fatigue fractures. Moreover, increasing the crown height space (CHS) can elevate tension in the peri-implant bone [3]. Although increasing the diameter of the implant can alleviate strain, it may not necessarily decrease bone stress under both axial and oblique loads [4]. The mechanical stress tends to concentrate in the areas of bone closest to the implant, gradually decreasing towards the outer regions. The highest stress occurs in the cortical bone areas immediately adjacent to the implant neck, with the maximum von Mises stress located inside the implant itself [5]. Implementing wider implants and reducing their number can help diminish stress in both the bone and prosthetic components [6]. When evaluating the survival rate of implants, it is crucial to consider implant length and diameter [7]. In assessing the survival rate of implants, factors such as implant length, diameter, shape, and position play a significant role in determining their long-term success and durability [8]. Nanotubes have emerged as a promising generation of advanced implant materials due to their biocompatibility with the biological environment. These unique properties make them well-suited for various implant applications, offering potential benefits for improved integration and long-term performance [9]. Materials such as titanium alloys, specifically TiAl6V4, can be utilized as they possess similar elastic moduli to bone [10]. While titanium implants are commonly used for their favorable mechanical properties and biocompatibility, it is essential to minimize porosity during manufacturing to ensure their long-term stability. The success of dental implants relies on surface characteristics and designs that promote osseointegration instead of porosity [11].

2. Methodology

The method for this study involved two primary steps. Initially, a dental implant design was crafted using drafting software, and the drawing was then imported into a simulation program. Figure 1 presents the design of Model 2 in both isometric and three different planes, providing an overview of the implant's geometric traits and their potential impact on its performance under diverse loading conditions. Subsequently, Model 1 was developed as a continuum model, where geometric features were formed using simulation software. Additionally, the design of the full body (free body diagram) for Model 2 was also created using the same approach, as depicted in Figure 2 (left) and (right). Following the creation of these models, simulations were conducted for both systems to investigate the behavior of the dental implant under various loading conditions.

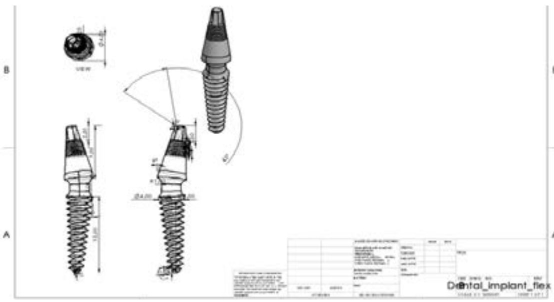

Figure 1: Displays the Design of Model 2 In Both Isometric and Three Different Planes

For the model setup, the probe was modeled as a linear elastic material, while the tissue was modeled using its own unique material properties. The properties of the polysilicon probe and tissue are as follows: Young's modulus [Pa], Poisson's ratio, and density [kg/m3]. The Young's modulus, Poisson's ratio, and density for the polysilicon probe are 1.69e11, 0.22, and 2320, respectively. The Young's modulus, Poisson's ratio, and density for the tissue are 1e4, 0.49, and 1080, respectively.

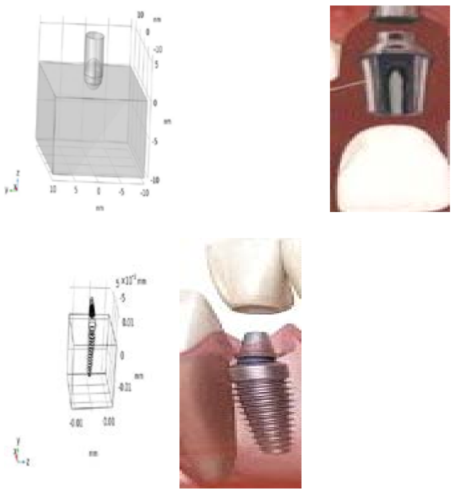

Figure 2: Shows Continuume Model (Top), Full-Body Model (Bottom)

Figure 2 illustrates the two models utilized in this study. The model on the top represents Model 1, a continuum model, while the model on the bottom depicts Model 2, a full-body model. This figure offers an overview of the two models employed to simulate the behavior of the dental implant under various loading conditions, facilitating a clearer understanding of their distinctions and similarities.

Table 1 outlines the geometric characteristics of the two models utilized in this study. Model 1 is a three-dimensional continuum model, whereas Model 2 is a three-dimensional full-body model. The table includes information on space dimensions, the number of domains, boundaries, edges, and vertices for each model. Model 1 features 3 space dimensions, 5 domains, 25 boundaries, 40 edges, and 22 vertices. In contrast, Model 2 encompasses 3 space dimensions, 3 domains, 133 boundaries, 316 edges, and 188 vertices. These statistics offer insights into the complexity of each model and underscore their differences concerning geometric attributes.

Description	Value of model 1	Value of mode 2
Space dimension	3	3
Number of domains	5	3
Number of boundaries	25	133
Number of edges	40	316
Number of vertices	22	188

Table 1: Shows Geometric Statistical

The dimensions of Model 1, which includes the dental implant, are as follows: Width 20mm, Depth 20mm, Height 10mm, and stem Radius 2mm and Height 5mm. Both the dental implant and tissue are made of polysilicon, with tissue having a density of 2320 kg/m^3, Young's modulus of 169e9 Pa, and Poisson's ratio of 0.22. The initial parameters for the simulation include an angle of indentation of 0[deg], applied pressure of P0 = 200 Pa, and a value of theta.

The equations used in this study describe the mechanics of a solid material under deformation. The equilibrium equation, 0 = V. s + Fv, describes the balance between external forces and internal stresses within the material. The equation S = Sinei + Sei relates the total stress to elastic and inelastic stress, while the equation Ɛ ei = Ɛ - Ɛ inel relates elastic and inelastic strain. The equation Ɛ inel = Ɛo + Ɛext + Ɛth + Ɛns + Ɛpi + Ɛcr + Ɛvp + Ɛve describes the inelastic strain due to various factors. The equations Sei = C: Ɛei and Sinei = So + Sext + S q relate stresses to elastic and plastic deformation. The equation Ɛ = ½ ((Vu)^2 + Vu) describes total strain in terms of the velocity gradient and rate of deformation. Finally, the equation C = C(E,υ) relates the stiffness tensor to elastic modulus and Poisson's ratio. Together, these equations provide a comprehensive understanding of the behavior of solid materials under stress and deformation.

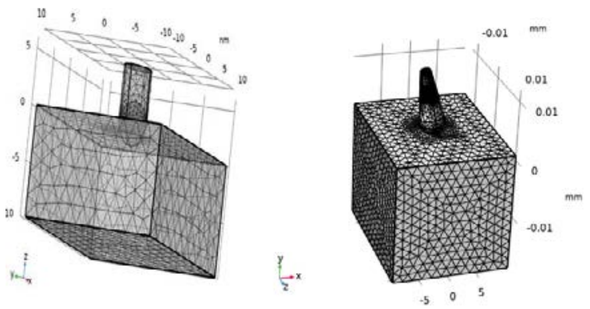

Figure 3: Shows Two Mesh Models

Figure 3 displays the mesh used for modeling both Model 1 (left) and Model 2 (right). The appropriate meshing of the dental implant is crucial for accurately modeling its behavior under various loading conditions, allowing for a more reliable and accurate simulation. By optimizing the mesh for each model, the simulation can provide insights into the implant's stability and long-term performance.

Table 2 presents the mesh statistics for both models, including information about the number of elements, nodes, and element types used in the simulation. These statistics provide insights into the level of detail and accuracy achieved in the meshing process. By optimizing the mesh, the simulation can accurately capture the behavior of the dental implant under various loading conditions, ensuring its stability and functionality in the long term.

Description model 1	Value	Description model 2	Value
Status	Complete mesh	Status	Complete mesh
Mesh vertices	2337	Mesh vertices	15573
Tetrahedra	11314	Tetrahedra	83383
Triangles	2166	Triangles	13052
Edge elements	223	Edge elements	2730
Vertex elements	22	Vertex elements	184
Number of elements	11314	Number of elements	83383
Minimum element quality	0.02658	Minimum element quality	0.004952
Average element quality	0.6451	Average element quality	0.6049
Element volume ratio	8.0558E-5	Element volume ratio	8.5845E-8
Mesh volume	4073 nm^3	Mesh volume	1.007E-5 mm^3

Table 2: Displays the Size Settings Used to Simulate Model 1 And Model 2

Including their descriptions, maximum and minimum element sizes, curvature factor, resolution of narrow regions, and maximum and element growth rates. These settings are crucial for accurately modeling the behavior of the dental implant under various loading conditions. By optimizing these parameters, the simulation can provide more reliable and accurate results, ensuring the implant's stability and durability.

Description model 1	**Value**	**Description model 2**	**Value**
Maximum element size	2	Maximum element size	0.003
Minimum element size	0.36	Minimum element size	5.4E-4
Curvature factor	0.6	Curvature factor	0.6
Resolution of narrow regions	0.5	Resolution of narrow regions	0.5
Maximum element growth rate	1.5	Maximum element growth rate	1.5

Table 3

Table 3 presents a detailed description of the mesh used for modeling the tissues surrounding the dental implant in both Model 1 (left) and Model 2 (right). This table includes information about the number of nodes and elements, as well as the mesh type and size distribution. Optimizing the mesh for the surrounding tissues is crucial for accurately modeling the behavior of the dental implant under various loading conditions. By achieving an appropriate mesh density, the simulation can provide more reliable and accurate results, ensuring the implant's stability and sustained functionality.

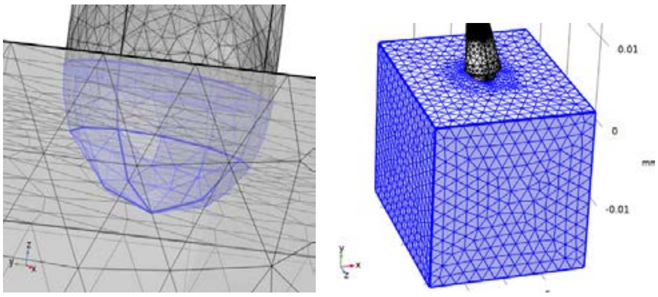

Figure 4: Shows Model 1(Left) And Right Mode 2

Figure 4 displays the meshed tissue surrounding the dental implant for both Model 1 (left) and Model 2 (right). The appropriate meshing of the tissue is essential for accurately modeling the behavior of the dental implant under various loading conditions, allowing for a more reliable and accurate simulation. By achieving an appropriate mesh density, the simulation can provide insights into the implant's stability and longevity.

Description model 1	**Value**	**Description model 2**	**Value**
Maximum element size	0.7	Maximum element size	0.00165
Minimum element size	0.03	Minimum element size	1.2E-4
Curvature factor	0.3	Curvature factor	0.4
Resolution of narrow regions	0.85	Resolution of narrow regions	0.7
Maximum element growth rate	1.35	Maximum element growth rate	1.4
Predefined size	Extra fine	Predefined size	Finer

Table 4

Table 4 provides a detailed description of the mesh used for modeling the dental implant in both Model 1 (left) and Model 2 (right). This table includes information about the number of nodes and elements, as well as the mesh type and size distribution. By optimizing the mesh for each model, the simulation can more accurately capture the behavior of the dental implant under various loading conditions, allowing for a better understanding of its stability and functionality.

Figure 5 presents a parametric sweep for theta, ranging from -60° to 15° to 60°, during the simulation to study the impact of dental implant rotation. The purpose of this analysis is to investigate the effects of rotation during chewing and its impact on the dental implant. Furthermore, Figure 6 illustrates the boundary loads for model 1 and model 2, respectively, on the left and right sides. These boundary loads are essential for simulating the behavior of the dental implant under different loading conditions and to assess its stability and durability.

Figure 7 illustrates the distribution of von Mises stress (N/m2) in Model 1 (left) and Model 2 (right). The von Mises stress is a measure used to predict yielding of materials under complex loading conditions, and it is represented in the figures to demonstrate the stress distribution in the respective models.

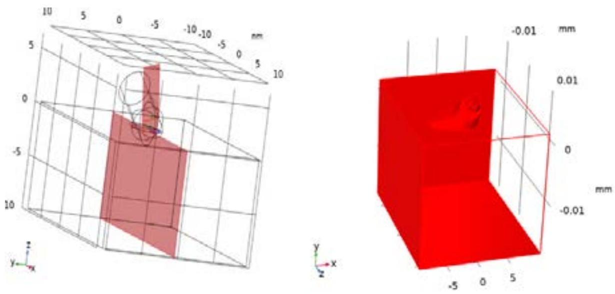

Figure 5: Shows Parameters Sweep for Theta, Range (-60°, 15°°, 60°) In Mode 1 (Left) And (Right) Model 2

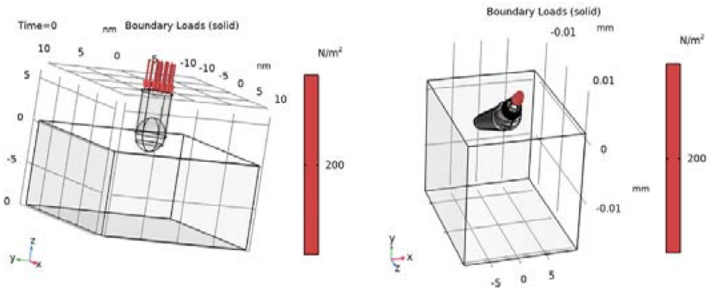

Figure 6: Shows Boundary Loads in Model 1 (Left) And (Right) Model 2

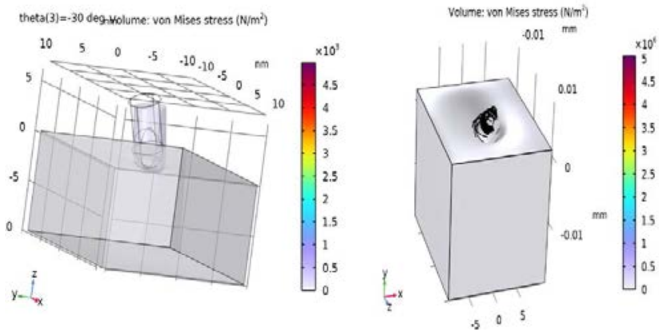

Figure 7: Shows Volume: Von Mises Stress (N/M2) In Model 1 (Left) And Model 2(Right)

Figure 8 illustrates the results of the continuum model, which shows the effects of rotating the dental implant at different theta angles, including 0°, -60°, 60°, and 15°. The figure depicts the impact of these rotations on the surface displacement magnitude (μm) in the tissue, as well as the changes in deformation shape resulting from changes in the angle of rotation.

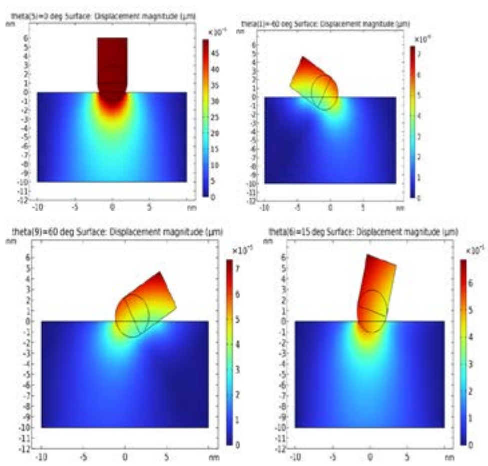

Figure 8: Show Surface: Posting in Different Angles with Displacement Magnitude (μM) of Model 1 in 2D

Figure 9 displays the effect of different angles of rotation on the surface of the dental implant, along with the associated displacement magnitude (μm), as depicted by the respective angles. The changes in deformation shape can significantly impact the dental implant's stability and functionality, as excessive deformation can lead to increased stress concentrations, localized failure of the implant, and surrounding bone tissue. Therefore, it is essential to understand the implant's deformation behavior under different angles of rotation to optimize its design and enhance its reliability and longevity. The figure displays dental implant angles ranging from 0° to 60°, including 15°, 45°, and shows the impact of increased deformation on the surrounding tissue.

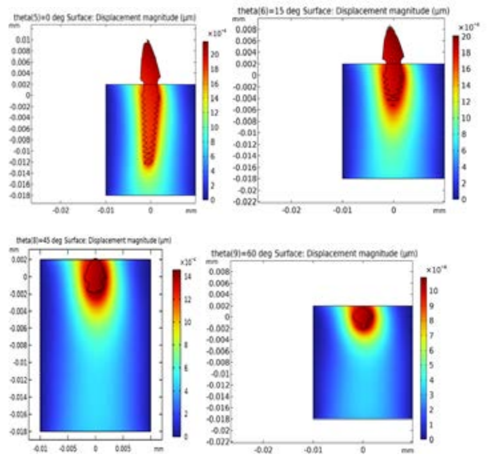

Figure 9: Show Surface: Positing in Different Angles with Displacement Magnitude (μm) of Model 2 in 2D

The analysis of model 1 reveals the relationship between von Mises stress (N/m2) and the angle of indentation, along with the displacement magnitude (μm) in the third coordinate. The stress distribution is symmetric for small angles, but it becomes asymmetric as the angle increases to 50°. However, the deformation remains symmetric around the angle of zero 0° for model 1, as depicted in Figure 10.

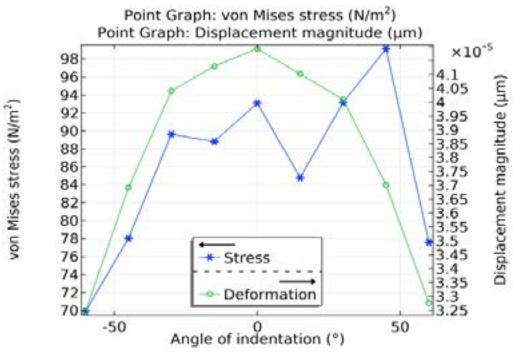

Figure 10: Shows Point Graph: Von Mises Stress (N/m2) Point Graph: Displacement Magnitude (μm) Model 1

The analysis of model 1 investigates the movement of a dental implant in the x-coordinate (nm) and von Mises stress (N/m2), as shown in Figure 11. The results demonstrate the effect of a range of rotations from -60° to -15° on the dental implant. The peak stress levels for positive angles of rotation shift towards the left side of zero (mm), while for negative angles, they shift towards the right side, as illustrated in Figure 11.

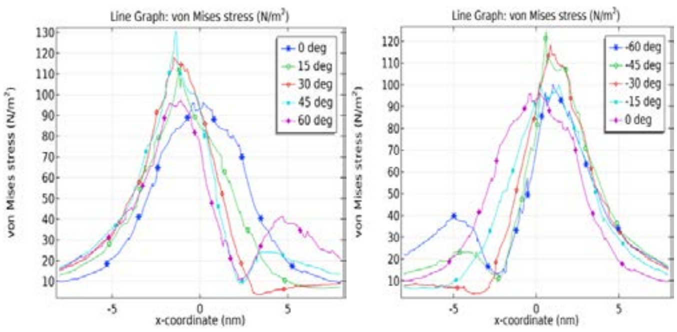

Figure 11: Shows Line Graph: Von Mises Stress (N/M2) With X-Coordinate in Model 1

In the y-coordinate (mm), the movement of the dental implant and von Mises stress (N/m2) are shown in Figure 12. The results illustrate the effect of a range of rotations from 60° to -60° on the dental implant. The peak stress levels for positive angles of rotation are in the middle of zero (mm), except for 30°, which is towards the right side. For negative angles of rotation, the peak stress levels are in the middle at zero (mm), as illustrated in Figure 12.

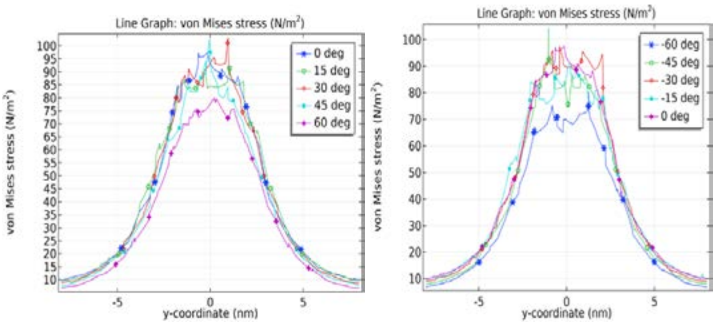

Figure 12: Shows Line Graph: Von Mises Stress (N/M2) With Y-Coordinate in Model 1

The analysis of model 2 reveals the relationship between von Mises stress (N/m2) and the angle of indentation, along with the displacement magnitude (µm) in the third coordinate. The stress distribution is symmetric around the angle of 0°, and it tends towards 0° when the angle increases to 50°. However, the deformation remains symmetric around the angle of zero 0° for model 2, as depicted in Figure 13.

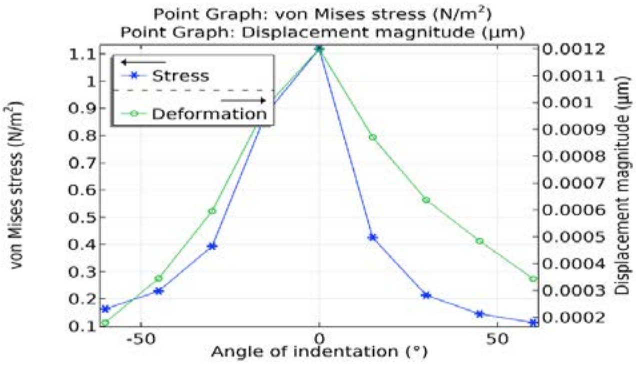

Figure 13: Shows Point Graph: Von Mises Stress (N/m2) Point Graph: Displacement Magnitude (µm) in Model 2

The analysis of model 2 investigates the movement of a dental implant in the x-coordinate (mm) and von Mises stress (N/m2), as shown in Figure 14. The results demonstrate the effect of a range of rotations from -60° to -15° on the dental implant. The peak stress levels for positive angles of rotation shift towards the right side of zero (mm), and for negative angles as well, as illustrated in Figure 14.

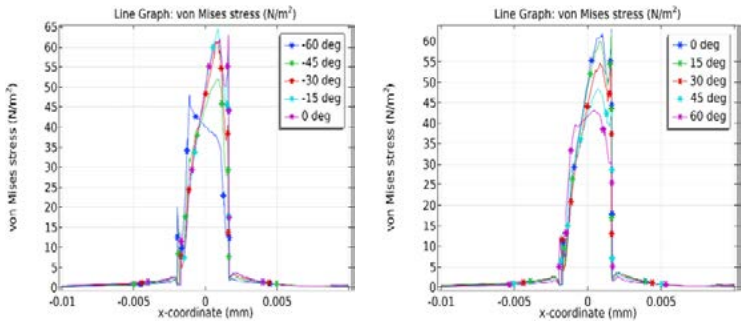

Figure 14: Shows Line Graph: Von Mises Stress (N/M2) With X-Coordinate in Model 2

In model 2, the movement of the dental implant and von Mises stress (N/m2) in the y-coordinate (mm) are shown in Figure 12. The results demonstrate the effect of a range of rotations from 60° to -60° on the dental implant. The peak stress levels for positive angles of rotation are observed in the middle of zero (mm), except for 15° and 30°, which are towards the left side. For negative angles of rotation, the peak stress levels are in the middle at zero (mm), except for -15° and -30°, which are towards the left side, as shown in Figure 15.

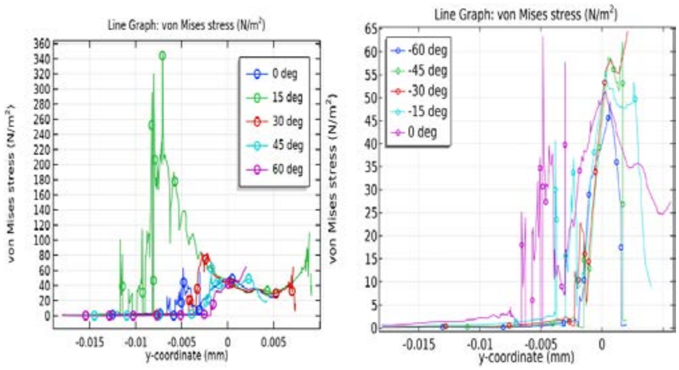

Figure 15: Shows Line Graph: Von Mises Stress (N/M2) With Y-Coordinate in Model 2

The analysis of model 2 investigates the movement of a dental implant in the z-coordinate (mm) and von Mises stress (N/m2), as shown in Figure 16. The results demonstrate the impact of a range of rotations from -60° to -15° on the dental implant. The peak stress levels for both positive and negative angles of rotation are observed around the zero angle of 0° (mm), as illustrated in Figure 16.

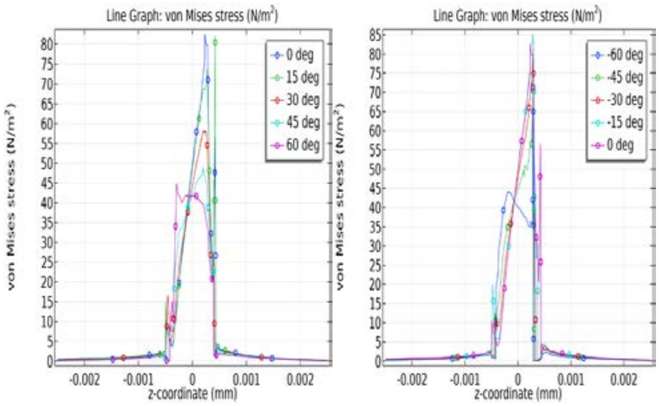

Figure 16: Shows Line Graph: Von Mises Stress (N/M2) With Z-Coordinate in Model 2

3. Conclusion

This study delves into the behavior of dental implants under stress, examining both a continuum model and a free body diagram of the solid state. The research indicates that stress applied to the implant cannot be precisely modeled using the continuum approach but can be better comprehended through the full body diagram created using an editor to depict the implant design. Boundary loads were applied to both models across a range of rotations from -60° to 60°, and the resulting stress distribution was analyzed. The outcomes demonstrate that simulating the full body diagram at different angles of rotation, both positive and negative, allows for an accurate prediction of the stress distribution and potential failure of the dental implant, encompassing both upper and lower stress levels. These findings suggest the potential development of an innovative simulation program to evaluate the anticipated stress and durability of tissue for this type of dental implant.

Funding Declaration
The authors declare no financial support for the research, authorship, or publication of this article. This research did not receive any specific grant from funding agencies in the public, commercial, or not-for-profit sectors.

Competing Interest Statement
The authors declare that they have no known competing financial interests or personal relationships that could have appeared to influence the work reported in this paper.

Availability of Data and Materials
All data and materials relevant to the manuscript are included within the article.

Author contributions
single author

Conflict of interest
The authors declare no conflict of interest.

Data availability statement
Data supporting these findings are available within the article

Sample availability
The authors declare no physical samples were used in the study.

References

1. Djebbar, N., Serier, B., Bouiadjra, B. B., Benbarek, S., & Drai, A. (2010). Analysis of the effect of load direction

on the stress distribution in dental implant. *Materials & Design, 31*(4), 2097-2101.

2. Paracchini, L., Barbieri, C., Redaelli, M., Di Croce, D., Vincenzi, C., & Guarnieri, R. (2020). Finite element analysis of a new dental implant design optimized for the desirable stress distribution in the surrounding bone region. *Prosthesis, 2*(3), 225-236.
3. Bulaqi, H. A., Mashhadi, M. M., Safari, H., Samandari, M. M., & Geramipanah, F. (2015). Effect of increased crown height on stress distribution in short dental implant components and their surrounding bone: A finite element analysis. *The Journal of Prosthetic Dentistry, 113*(6), 548-557.
4. Meimandi, M., Ardakani, M. R. T., Amid, R., Motlagh, A. M., & Beheshti, S. (2018). Comparison of stress and strain distribution around splinted and nonsplinted 6-mm short implants in posterior mandible: a finite element analysis study. *Implant Dentistry, 27*(1), 74-80.
5. Merdji, A., Bouiadjra, B. B., Chikh, B. O., Mootanah, R., Aminallah, L., Serier, B., & Muslih, I. M. (2012). Stress distribution in dental prosthesis under an occlusal combined dynamic loading. *Materials & Design (1980-2015), 36,* 705-713.
6. Silva-Neto, J. P. D., Pimentel, M. J., Neves, F. D. D., Consani, R. L. X., & Santos, M. B. F. D. (2013). Stress analysis of different configurations of 3 implants to support a fixed prosthesis in an edentulous jaw. *Brazilian Oral Research, 28,* 67-73.
7. Raikar, S., Talukdar, P., Kumari, S., Panda, S. K., Oommen, V. M., & Prasad, A. (2017). Factors affecting the survival rate of dental implants: A retrospective study. *Journal of International Society of Preventive and Community Dentistry, 7*(6), 351-355.
8. French, D., Larjava, H., & Ofec, R. (2015). Retrospective cohort study of 4591 Straumann implants in private practice setting, with up to 10-year follow-up. Part 1: multivariate survival analysis. *Clinical oral implants research, 26*(11), 1345-1354.
9. Hazan, R., Sreekantan, S., Mydin, R. B. S., Abdullah, Y., & Mat, I. (2016, January). Study of TiO2 nanotubes as an implant application. *In AIP conference proceedings* (Vol. 1704, No. 1). AIP Publishing.
10. Deing, A., Luthringer, B., Laipple, D., Ebel, T., & Willumeit, R. (2014). A porous TiAl6V4 implant material for medical application. *International Journal of Biomaterials, 2014*(1), 904230.
11. Marin, E., Fusi, S., Pressacco, M., Paussa, L., & Fedrizzi, L. (2010). Characterization of cellular solids in Ti6Al4V for orthopaedic implant applications: Trabecular titanium. *Journal of the Mechanical Behavior of Biomedical Materials, 3*(5), 373-381.